Macromolecules

pubs.acs.org/Macromolecules
Article

Design Chemical Structures of CO_2-Derived Poly(cyclohexene carbonate) Copolymers to Mediate Intra-/Intermolecular Interactions with Strong Hydrogen-Bonded Donor Homopolymer

Yen-Ling Kuan, Chih-Wei Chu, Wei-Ting Du, and Shiao-Wei Kuo*

Cite This: *Macromolecules* 2025, 58, 1090−1102

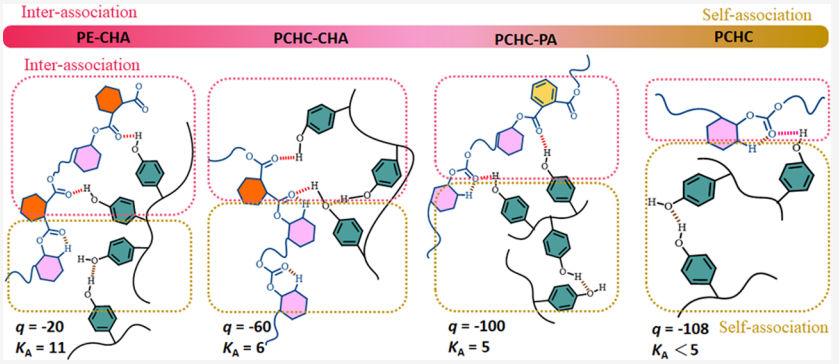

ABSTRACT: The ring opening copolymerization (ROCOP) of CO_2-based poly(carbonate-*co*-ester) (PC-*co*-PE) copolymers was synthesized by cyclohexene oxide (CHO), anhydrides (AH), and carbon dioxide (CO_2) with various contents of AH. Herein, phthalic anhydride and 1,2-cyclohexanedicarboxylic anhydride were chosen for prepared poly(cyclohexene carbonate-*co*-cyclohexane carboxylate) (PCHC-CHA) and poly(cyclohexene carbonate-*co*-phthalate) (PCHC-PA). Polycarbonate-*co*-polyester and polyester copolymers possess strong intramolecular H-bonding interactions on the polycarbonate (PC) or polyester (PE) segments, which was confirmed by two-dimensional Fourier transform infrared (2D FTIR) spectroscopy analyses. Compared to the PC segment, the OH units of poly(vinylphenol) (PVPh) preferred to form intermolecular hydrogen bonding with the polyester segment and possess a higher intermolecular association equilibrium constant (K_A). The trend of intermolecular H-bonded strength was PVPh/PE-CHA > PVPh/PCHC-CHA > PVPh/PCHC-PA > PVPh/PCHC binary blends. Adjusting the PC % and PE % could improve the intra-/intermolecular hydrogen bonding ratio on the PVPh/PC-*co*-PE binary blend, which could be observed in the change of the q value (q value generally corresponds to the H-bonding strength of the miscible polymer blend based on the Kwei equation) from DSC analyses.

INTRODUCTION

Plastic is ubiquitous, offering convenience in several applications, including packaging, medical equipment, and transportation. However, plastic pollution has adverse impacts on both the environment and human health.[1,2] Plastic production has expanded more than 200 times in the last 80 years, from 1.5 million tons to 460 million tons.[3−5] The use of plastics is predicted to increase globally as urbanization progresses. Polyester stands out as one of the most prevalent plastic materials with excellent mechanical and chemical properties, and its thermoplastic makes it suitable for diverse applications.[6−8] Lactones are one of the materials used to form polyester, and polymerization of lactones was reported in three kinds of polymerization methods: step-growth polymerization, chain-growth polymerization, and ring-opening copolymerization (ROP); lactones are prone to byproducts or are difficult to functionalize, which limits their production in large quantities.[9−11]

Plastics offer convenience but also pose a significant environmental burden. A large volume of waste plastics is not recyclable, leading to the release of plastic particles into the environment. The manufacturing process of plastics generates carbon dioxide (CO_2), contributing to global warming and climate change.[12] Carbon capture and utilization (CCU) is a key approach to reducing carbon emissions.[13−20] By copolymerizing carbon-negative materials, it effectively lowers

Received: September 21, 2024
Revised: December 8, 2024
Accepted: December 18, 2024
Published: December 31, 2024

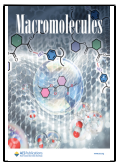

Scheme 1. Synthesis of the CHO/AH/CO_2 Copolymers of PCHC, PE-CHA, PCHC-CHA, and PCHC-PA

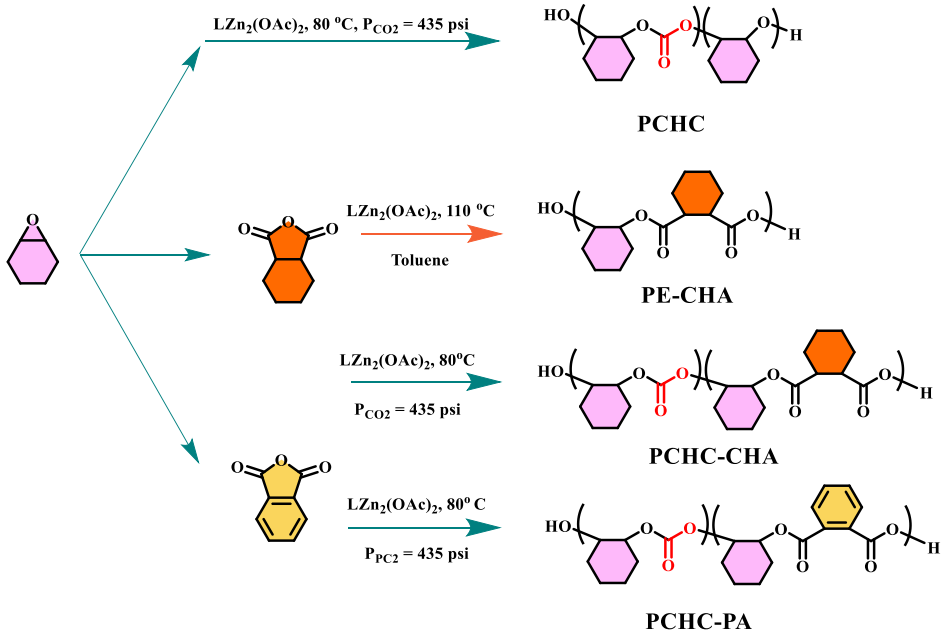

atmospheric CO_2 levels.[21] Furthermore, carbonate-based copolymers demonstrate good biodegradability, allowing them to decompose in the environment and successfully complete the carbon cycle.[22−24] The ring opening copolymerization (ROCOP) of CO_2-based copolymers was the chosen monomer from bioderived resources, which gives polycarbonate good biocompatibility and biodegradability, and attracted a lot of attention. Typically, CO_2-based copolymers with carbonate groups adjust the kind of monomer to improve chemical and physical properties, making them a sustainable alternative for commercial applications.[25−27]

The previous work was reported by copolymerization of epoxides with CO_2 such as propylene oxide (PO) or cyclohexene oxide (CHO) to synthesize biodegradable polycarbonate to form poly(propylene carbonate) (PPC) or poly(cyclohexene carbonate) (PCHC) that could the effectively decrease emission of greenhouse gas.[28,29] To enhance the thermal or mechanical properties of PPC or PCHC, blending these copolymers with poly(lactic acid) (PLA), poly(methyl methacrylate) (PMMA), cellulose, and starch has been proposed.[30−34] Recently, we chose cyclohexene oxide as the main monomer to copolymerize with CO_2 to form poly(cyclohexene carbonate) (PCHC) copolymers and investigated the H-bonding interaction of PCHC blended with PVPh.[35,36] Poly(vinylphenol) (PVPh) homopolymer is a strong hydrogen-bond donor and can exhibit miscible behavior with various hydrogen-bond acceptor homopolymers or copolymers. The strength of these hydrogen bonds has been widely investigated in previous studies, making it a valuable model for understanding hydrogen-bond interactions with CO_2-based copolymers.[37−46] Therefore, the H-bonding interaction of the PCHC/PVPh binary blend should be investigated. The pure PCHC had intramolecular H-bonding interaction based on 2D-FTIR analyses[47] and results in relatively weaker intermolecular H-bonding interaction with OH groups of PVPh.[35] Therefore, the intermolecular association equilibrium constant (K_A < 5) was determined based on the Painter−Coleman association model (PCAM)[48] and the q value of PVPh/PCHC binary blend was −108 based on the Kwei equation.[49]

To expand the applications of CO_2-based copolymers in different fields, more diversified materials are needed. Here, the thermal properties of these copolymers were changed by using different anhydrides for copolymerization. Anhydrides and epoxides produce ester groups, and the addition of polyester [polyester (PE) segment] to polycarbonate [polycarbonate (PC) segment] would affect the H-bonding interaction on the copolymer, as shown in Scheme 1. Then, the polyester segment could enhance the intermolecular H-bonding interactions with PVPh blends.

EXPERIMENTAL SECTION

Materials. Cyclohexene oxide (98%) and toluene were stirred over calcium hydride for 12 h and distilled under reduced pressure prior to use. Dichloromethane (Acros), toluene (Acros), ethyl ether anhydrous (Acros), tetrahydrofuran (Acros), methanol (Acros), poly(4-vinylphenol) (Sigma-Aldrich), phthalic anhydride (SHOWA), magnesium sulfate anhydrous (SHOWA), 1,2-cyclohexanedicarboxylic anhydride (≥97%, Alfa-Aesar), hydrochloric acid (Alfa-Aesar), and chloroform (Alfa-Aesar) were purchased and used without further purification. High-purity CO_2 (>99.999%) was purchased from Hsin E-Li Co., Ltd. The catalyst $LZn_2(OAc)_2$ and poly(cyclohexene carbonate) (PCHC) copolymer were prepared following the previously recorded procedures.[35]

Copolymerization of CO_2, CHO, and Anhydrides (PCHC-PA and PCHC-CHA). Poly(cyclohexene carbonate-*co*-phthalate) (PCHC-PA) was synthesized by ROCOP of CO_2, CHO, and PA. The PA (1.75 g, 0.01 mol) and catalyst $LZn_2(OAc)_2$ (0.0732 g, 0.0001 mol) were dried in the autoclave under 80 °C and vacuum for 6 h. The autoclave was purged with CO_2, CHO (12 mL, 0.1 mol) was injected into the reactor at room temperature, and the mixture was reacted under 110 °C and 435 psi of P_{CO_2} for 20 h. When the reaction finished, the reactor was put into an ice bath to cool down and release the unreacted CO_2, then DCM was added into the reactor to dissolve the product, and methanol was added to terminate the reaction. The catalyst was removed through extraction with 5 wt % HCl solution, and the moisture was removed through $MgSO_4$. The solution was added dropwise into a large amount of cold methanol to obtain the powder through reprecipitation many times. The product was dried

https://doi.org/10.1021/acs.macromol.4c02295
Macromolecules 2025, 58, 1090−1102

Table 1. Ring Opening Polymerization of CHO/AH/CO_2 Catalyzed by $LZn_2(OAc)_2$[a]

entry	polymer	conv.[b] (CHO %)	conv.[b] (AH %)	% PC[c]	% PE[c]	% PCHO[c]	TON[d]	TOF (h^{-1})[e]	% select[f]	T_g (°C)[g]	M_n[h]	$Đ$[h]
1	PCHC			98.4		1.6			>99.9	108	21,900	1.72
2	PCHC-PA50	65.6	>99	62.5	8.5	29	61.1	3.1	92.4	72	4200	1.10
3	PCHC-PA100	78.0	98.9	73.2	10.8	16.0	70.7	3.5	87.2	76	3100	1.07
4	PCHC-PA200	68.7	97.5	40.1	30.7	29.2	89.7	4.5	85.8	55	2900	1.05
5	PCHC-PA500	>99	100	0	100	0	216.9	10.6		54	1600	1.10
6	PCHC-CHA50	65.2	>99	88.7	11.3	<0.1	72.1	3.6	>99	102	12,600	1.26
7	PCHC-CHA100	65.0	96.1	74.6	17.5	7.9	81.5	4.1	98.9	80	11,100	1.50
8	PCHC-CHA200	77.0	>99	60.5	36.4	3.1	106.4	5.3	95.6	97	8200	1.18
9[i]	PCHC-CHA100	58.7	97.9	67.1	22.4	10.4	26.6	1.3	>99	87	5500	1.10
10[j]	PE-CHA	65.0	96.1		>99	<1	168.7	8.4		83	4300	1.04

[a]Polymerization conditions: [CHO]/[AH]/[cat.] = 1000:*X*:1. [b]Determined by ^{1}H NMR analysis of the crude product. [c]PC = polycarbonate, PE = polyester, PCHO = polyether. The compositions were estimated according to the ^{1}H NMR spectra. [d]Turnover number = polymer (g)/catalyst (g). [e]Turnover frequency = TON/time (hours). [f]Selectivity toward polymer over cyclohexene carbonate calculated from the ^{1}H NMR spectrum. [g]Determined by DSC analysis. [h]Determined by GPC in DMF, calibrated with narrow molar mass polystyrene standards (Figure S1). [i]Reaction time = 10 h. [j]Reaction condition: [CHO]/[AH]/[cat.] = 1000:800:1 in the absence of CO_2.

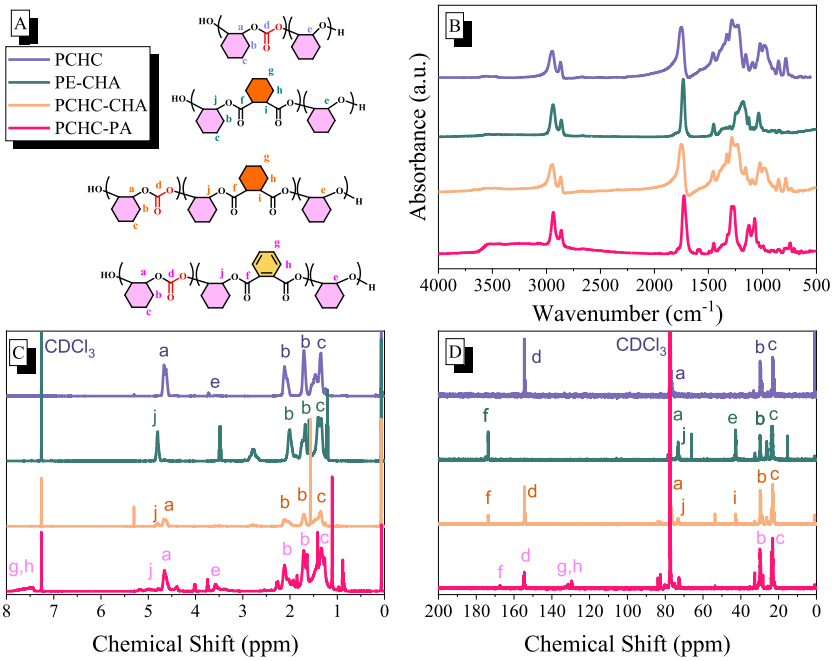

Figure 1. Synthesis of the PCHC-PA, PCHC-CHA, and PE-CHA copolymer. (A) Scheme of structure, (B) FTIR, (C) ^{1}H NMR, and (D) ^{13}C NMR spectra.

under 40 °C with high vacuum for 24 h. ^{1}H NMR (500 MHz, $CDCl_3$, δ, ppm): 4.63 ($CyCHOCO_2$), 3.55 (CyCHOC), 7.49 (ArH), 1.26–2.26 ($CyCH_2$). ^{13}C NMR (125 MHz, $CDCl_3$, δ, ppm): 154.5 (CyCHOC), 129.4 (ArH), 167.2 (OCAr), 21.9–30.7 ($CyCH_2$). FTIR (KBr, cm^{-1}): 1749 (C═O).

Furthermore, the same procedure and same molar ratio were used to synthesize poly(cyclohexene carbonate-*co*-cyclohexane carboxylate) (PCHC-CHA). ^{1}H NMR (500 MHz, $CDCl_3$, δ, ppm): 4.63 ($CyCHOCO_2$), 2.77(OCCyHCO), 3.55 (CyCHOC), 1.26–2.26 ($CyCH_2$). ^{13}C NMR (125 MHz, $CDCl_3$, δ, ppm): 154.5 (CyCHOC), 173.7 (OCCyHCO), 42.7 (OCCyHCO), 21.9–30.7 ($CyCH_2$). FTIR (KBr, cm^{-1}): 1749 (C═O).

Copolymerization of CHO and 1,2-Cyclohexanedicarboxylic Anhydride (PE-CHA). In a two-neck round-bottom flask, 1,2-cyclohexanedicarboxylic anhydride (12.19 g, 0.08 mol) and $LZn_2(OAc)_2$ (0.0732 g, 0.0001 mol) were introduced and dried under 80 °C on the vacuum for 3 h. Toluene (12 mL) and CHO (12 mL, 0.1 mol) were added to the flask and stirred with a magnetic stirring bar. Nitrogen bubbled through the round-bottom flask, and the solution reacted under 110 °C for 20 h. After the polymerization, DCM was added into the flask to dissolve the product and quenched in methanol. The catalyst was removed through extraction with 5 wt % HCl solution, and the moisture was removed by $MgSO_4$. Then, the product was reprecipitated with DCM/methanol. The white powder was dried in a vacuum oven at 60 °C. ^{1}H NMR (500 MHz, $CDCl_3$, δ, ppm): 4.79 (CyCHO), 2.78 (CyCHOC), 1.26–2.26 ($CyCH_2$). ^{13}C NMR (125 MHz, CDCl3, δ, ppm): 173.7 (OCCyHCO), 73.1 (CyCO), 42.7 (OCCyHCO), 21.9–30.7 ($CyCH_2$). FTIR (KBr, cm^{-1}): 1732 (C═O).

Preparation of Binary Polymer Blends. The polymer blends were prepared by adding certain weight of copolymers and PVPh in flask and then using THF to dissolve to obtain 5 wt % solution. The solvent evaporated under room temperature for 3 days, and then the flask was put into the vacuum oven at 40 °C for 3 days.

RESULTS AND DISCUSSION

Terpolymerization of Cyclohexene Oxide, Anhydrides, and CO_2 Block Copolymers. Terpolymerizations of poly(carbonate-*co*-ester) copolymers from CO_2, cyclo-

https://doi.org/10.1021/acs.macromol.4c02295
Macromolecules 2025, 58, 1090−1102

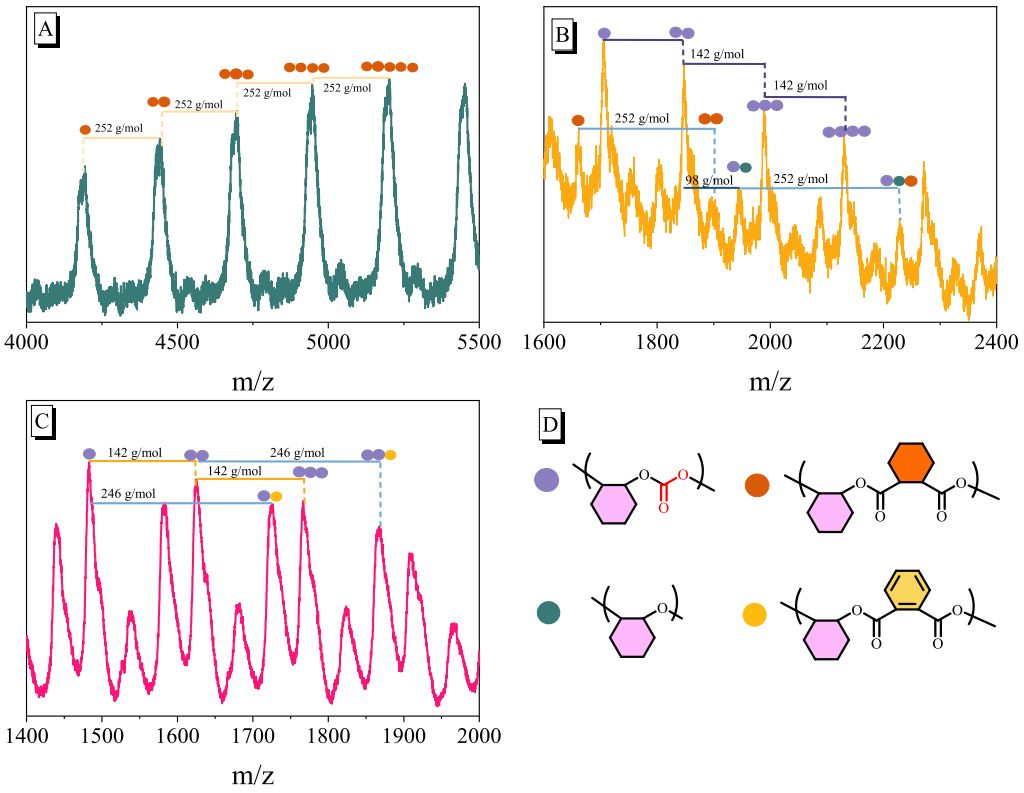

Figure 2. (A–C) MALDI-TOF mass of the CHO/AH and CHO/AH/CO_2 copolymer: (A) PE-CHA, (B) PCHC-CHA, (C) PCHC-PA100; and (D) structure of the copolymer repeat unit.

hexene oxide, and anhydrides were investigated (Table 1), and the terpolymerizations were carried out with aromatic PA and aliphatic CHA to different strengths of intermolecular hydrogen bonding on the binary blends. Moreover, alternating polycarbonate (PCHC) and polyester (PE-CHA) were synthesized by copolymerization and blended with PVPh as research of intra-/intermolecular hydrogen bonding, compared to the poly(carbonate-*co*-ester). Accordingly, terpolymerization was conducted under a pressure of 440 psi of CO_2 at 80 °C, and the ratio of monomer was [CHO]/[AH]/[cat.] = 1000:*X*:1. The characteristic peaks of polycarbonate and polyester were detected by the ^{1}H NMR spectra, and typical peaks of polyether units appeared at around 3.5 ppm. The peak a at 4.6 ppm corresponds to the cyclohexyl CH of polycarbonate PCHC units on the backbone, and the peak j at 4.7–4.8 ppm corresponds to the cyclohexyl CH of polyester units on the main chain (Figure 1C). The compositions of polyester and polycarbonate could be calculated by the integral area of NMR, based on the ratio of the two peaks a and j. Furthermore, the carbon signals of the C═O group of pure PCHC units and polyester units were detected at 154 and 167–173 ppm in the ^{13}C NMR spectrum, respectively (Figure 1D).

A series of experiments were carried out with different ratios of PA/CHA to CHO to explore the change of polyester and polycarbonate units on the poly(carbonate-*co*-ester). Even when loading of PA increased, PA conversions were still up to 97%, and it was observed that PE % was raised, and the PC % was dramatically decreased (entries 2–4, Table 1). The feeding ratio of PA to CHO to 200:1000 resulted in the formation of a copolymer with 30% of polyester and 40% of polycarbonate after 20 h of reaction for PA conversion reached 97.5%. Thus, the presence of PA caused lower conversions of CHO, in agreement with the literature results due to PA being more rapidly consumed than CHO; with PA being consumed, the reaction gradually becomes sticky, indicating results of lower CHO conversions.[50] With the feeding ratio of PA to CHO up to 500:1000, copolymer only had a polyester segment, and CHO was difficultly reacted with CO_2 on the viscid mixture (entry 5, Table 1). It was obvious that reactivity of PA was higher than that of CO_2, and the one end of copolymer was enriched with ester units and the other end with carbonate units and ether units. Depending upon the above-mentioned experiments, the synthesis of block poly(carbonate-*co*-ester) copolymers is used as additive PA.

In addition to attempts at copolymerizing aromatic PA, aliphatic CHA was terpolymerized with CHO and CO_2. Initially, the ratio of CHA to CHO was the same as that of PA to CHO, resulting in changes to the polyester and polycarbonate segments similar to those observed in PCHC-PA copolymers. Subsequently, the experiment was conducted for a shorter duration to determine whether the reactivity of CHA was indeed higher than that of CO_2. Ultimately, the conversion of CHA reached nearly 99%, with the reaction time reduced from 20 to 12 h (entry 9, Table 1). This indicates that the PCHC-CHA copolymers are also tends to blocky copolymers, similar to PCHC-PA.[51] On the other hand, polyester PE-CHA was formed by CHO and CHA at 80 °C without the presence of CO_2. The resulting PE-CHA copolymer was composed almost entirely of polyester segments, with only about 1% of polyether units that could be considered negligible (entry 10, Table 1).

The FTIR spectra of copolymers are shown in Figure 1B, with the signal of the C═O group of polycarbonates at 1750 cm^{-1} and the C═O group of polyester at ca. 1740 cm^{-1}. The single C═O peak was seen because the C═O signals of the

https://doi.org/10.1021/acs.macromol.4c02295
Macromolecules 2025, 58, 1090–1102

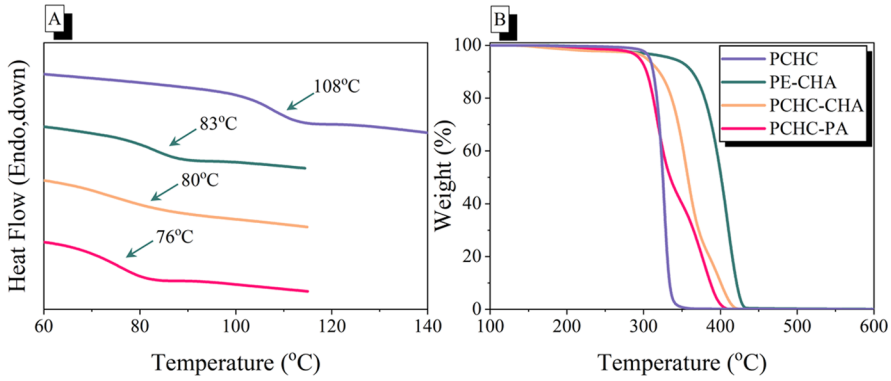

Figure 3. (A) DSC curves and glass transition temperatures of the CO_2-based copolymer and (B) thermogravimetric curves of the CO_2-based copolymer.

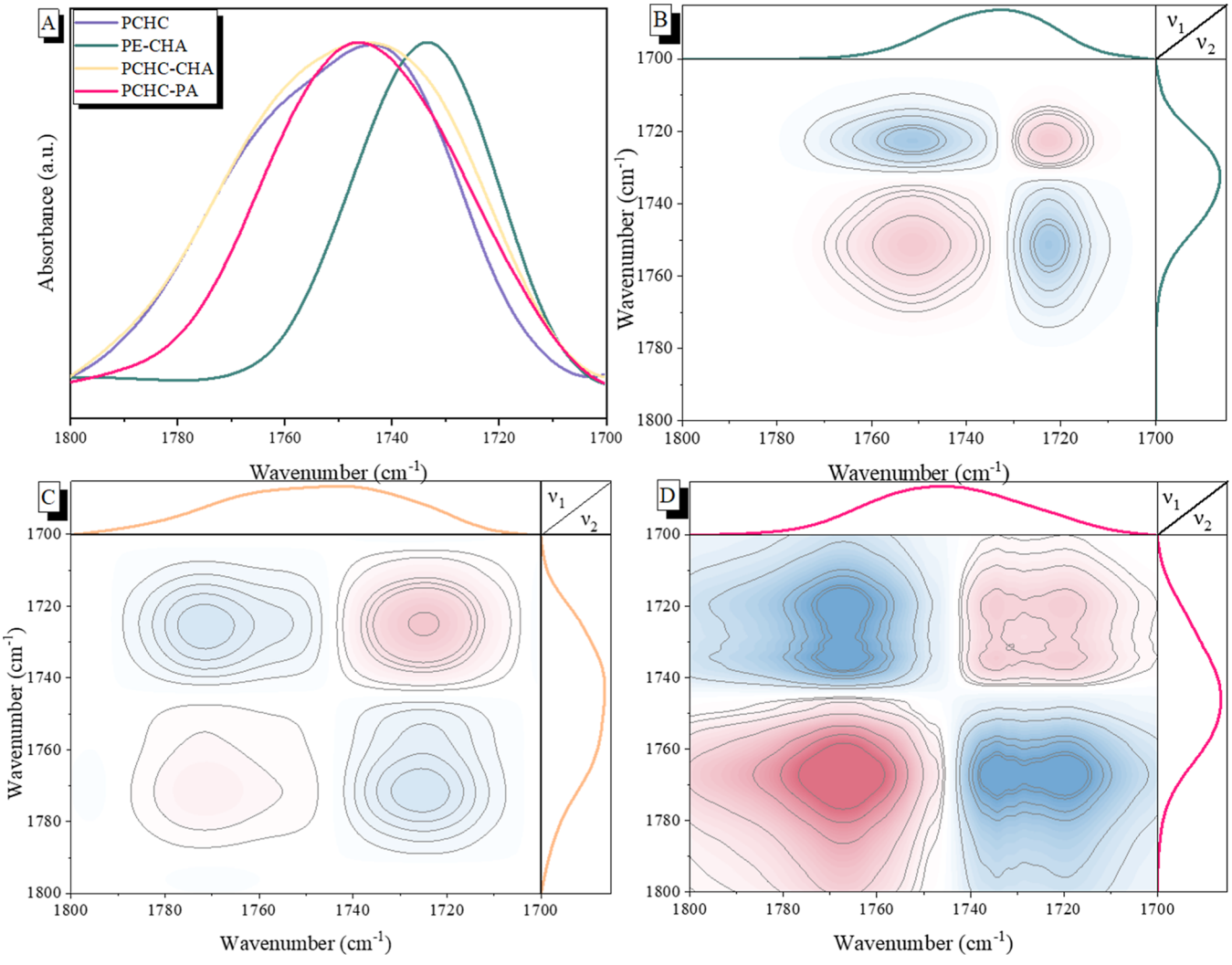

Figure 4. (A) FTIR spectra of C═O group and (B,C) corresponding 2D FTIR synchronous correlation maps. (B) PE-CHA, (C) PCHC-CHA, and (D) PCHC-PA.

PCHC-AH which included C═O of polycarbonate and polyester signals were closely overlapped.

Matrix-assisted laser desorption/ionization time-of-flight mass spectroscopy (MALDI-TOF) was conducted to further analyze the composition of the copolymers, for which polyester/polycarbonate segments were observed (Figure 2). The pure PCHC had regular repeat unit of ca. 142 g/mol, which was one CHO unit plus a CO_2 unit (Figure S2). A series of copolymer signals with regular repeat intervals (ca. 142 g/mol equal to one PCHC unit) were observed in the mass spectra of PCHC-CHA and PCHC-PA; there was a difference of ca. 252 g/mol, which was equal to one PE-CHA unit (Figure 2A,B). In addition, it was found that PCHC-PA copolymer showed similar results to PCHC-CHA, including

https://doi.org/10.1021/acs.macromol.4c02295
Macromolecules 2025, 58, 1090−1102

Scheme 2. Intramolecular Hydrogen Bonding Strength of PCHC, PE-CHA, PCHC-CHA, and PCHC-PA Copolymers

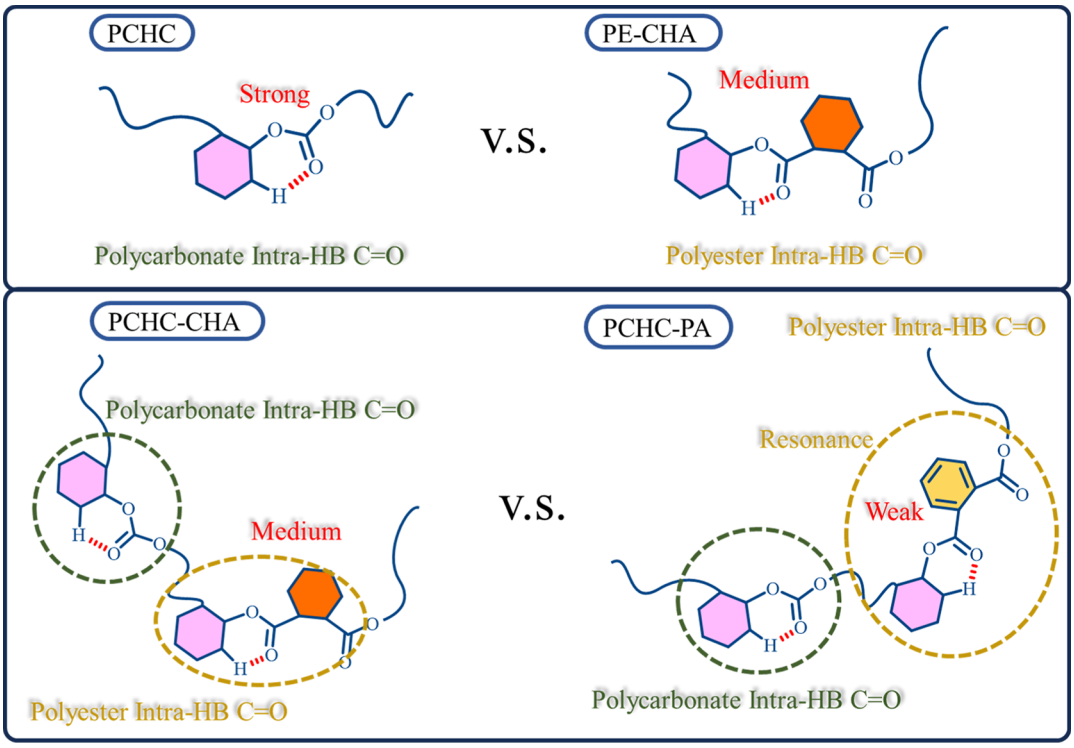

ca. 142 g/mol of interval for PCHC unit and ca. 246 g/mol of interval for the PE-PA unit (Figure 2C). From the above results, it could be confirmed that the anhydride has successfully formed a copolymer with the CHO monomer and CO_2.

The thermal properties of these copolymers were measured by DSC and TGA analyses (Figure 3). Pure PCHC synthesized from CHO and CO_2 exhibited the highest T_g value of 108 °C. However, when CO_2 is replaced with CHA, the T_g decreases due to the higher free volume associated with CHA compared to that of CO_2. In addition, PCHC-CHA and PCHC-PA copolymers showed T_g values of 80 and 76 °C, respectively. Compared to the pure PCHC copolymers, both PCHC-CHA and PCHC-PA had a lower T_g value. This reduction can be attributed to incorporation of the PC segment into the polyester segment, which reduced the intramolecular hydrogen bonding interaction and increased the free volume of copolymers (Figure 3A).

TGA of these copolymers is provided in Figure 3B. The PCHC-PA copolymer showed the lowest thermal stability; the temperature at 5% weight loss (T_{d5}) was 294 °C with two-step degradation profiles. The first stage of weight loss was the segment of polycarbonate, and the second stage was that of polyester. Similarly, PCHC-CHA also had two-step degradation profiles. This finding shows that both PCHC-PA and PCHC-CHA tend to be blocky copolymers. On the other hand, PCHC and PE-CHA were fully alternating copolymers (PCHO %).[52] However, we found that TGA and DSC had different trends, PE-CHA exhibited good thermal properties, and the addition of segment of polyester helped improve the thermal stability of PCHC.[53,54]

The strength of hydrogen bonding of the C═O groups of these copolymers was figured out through the FTIR spectra (Figure 4A). PE-CHA has free C═O groups and intramolecular hydrogen-bonded C═O groups formed; PCHC not only has free C═O groups but also intramolecular hydrogen-bonded C═O groups from polycarbonate.[35] Therefore, the full width at half-maximum (fwhm) about the C═O signal of PE-CHA was relatively narrower ($W_{1/2}$ = 30 cm^{-1}) compared to that of PCHC ($W_{1/2}$ = 49 cm^{-1}); while the C═O signal of PCHC-CHA copolymer ($W_{1/2}$ = 53 cm^{-1}) has a relative broader peak than that of PCHC copolymer because of the combination of polycarbonate and polyester segments in PCHC-CHA copolymer, where PCHC only possesses a polycarbonate segment. However, the full width at half-maximum of C═O of PCHC-PA ($W_{1/2}$ = 43 cm^{-1}) was smaller than that of PCHC-CHA because of the resonance of the benzene ring, which stabilizes the structure and results in fewer intramolecular hydrogen bonding being formed, as shown in Scheme 2.[55]

To clarify the strength of hydrogen bonding of the C═O groups of these copolymers easily, 2D-FTIR was employed. The synchronous correlation maps for the C═O signal was displayed at 1700−1800 cm^{-1}, as shown in Figures S3 and 4B,D. The signals of the intramolecular hydrogen-bonded C═O unit and free C═O units for pure PCHC appeared at 1735 and 1763 cm^{-1}, respectively; the negative cross-peaks (blue color) were observed for signals at 1763 and 1735 cm^{-1}, demonstrating that these two absorptions varied in the opposite direction (one is increased and the other is decreased), as shown in Figure S3.[35] Furthermore, the intramolecular hydrogen bonding and free C═O units of PE-CHA were located at 1720 and 1750 cm^{-1}, respectively; a similar result of the negative cross-peaks was observed at 1720 and 1750 cm^{-1}. PCHC-CHA and PCHC-PA copolymers exhibited a similar situation; the intramolecular hydrogen bonded and free C═O groups presented negative cross-peaks. However, the range of intramolecular hydrogen-bonded C═O units for PCHC-CHA copolymers was from 1710 to 1740 cm^{-1}, due to the signals being close between intramolecular

https://doi.org/10.1021/acs.macromol.4c02295
Macromolecules 2025, 58, 1090−1102

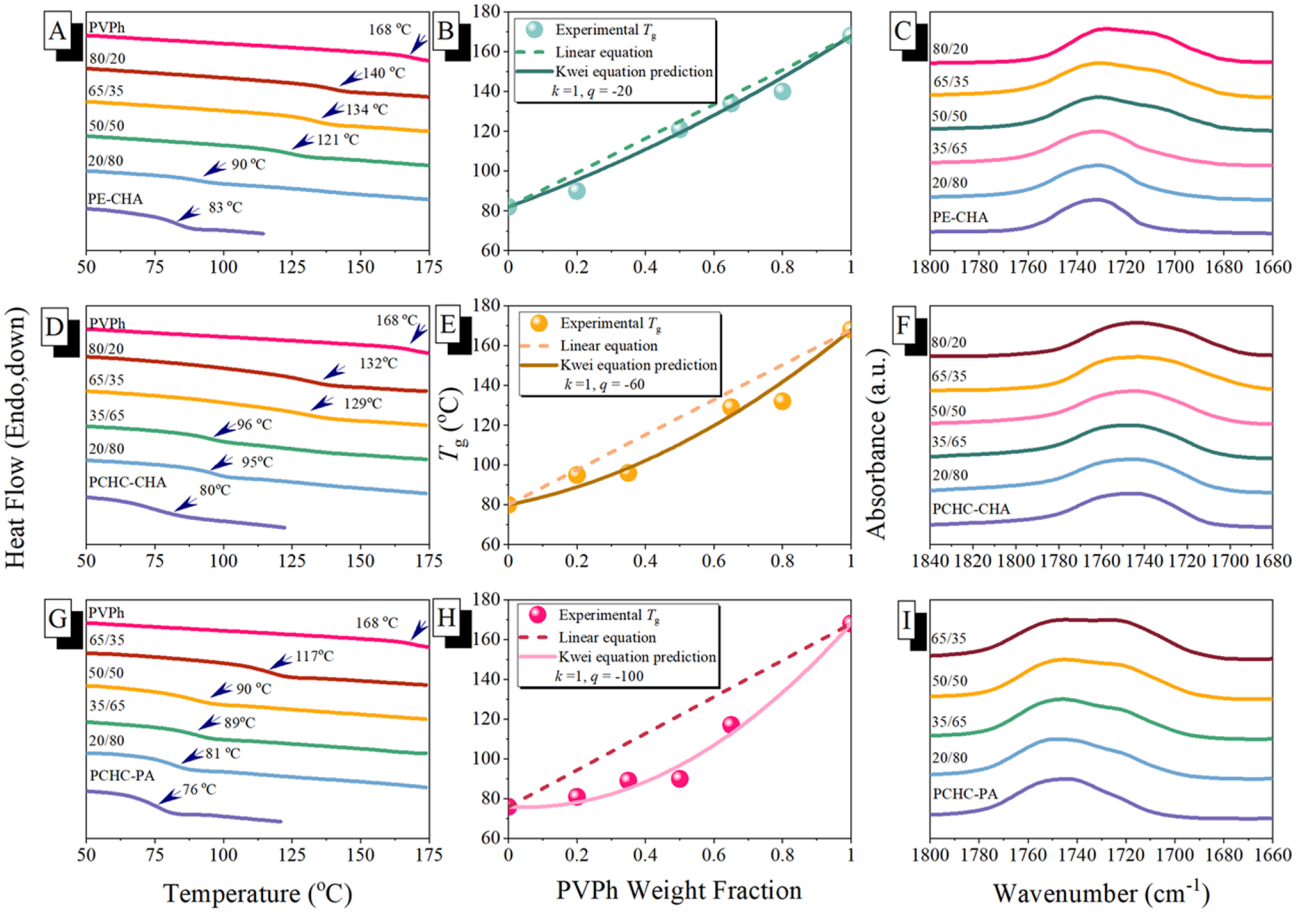

Figure 5. (A–C) PE-CHA100 copolymer: (A) DSC, (B) Kwei equation, and (C) C═O of FTIR; (D–F) PCHC-CHA100 copolymer: (D) DSC, (E) Kwei equation, and (F) C═O of FTIR; (G–I) PCHC-PA100 copolymer: (G) DSC, (H) Kwei equation, and (I) C═O of FTIR.

hydrogen bonded C═O units of polycarbonate and polyester segment; thus one signal was observed. Similarly, the results of the synchronous correlation map of PCHC-PA showed a similar phenomenon with PCHC-CHA, but PCHC-PA clearly distinguishes two absorption bands of intramolecular hydrogen-bonded C═O units at 1735 and 1720 cm^{-1}, corresponding to the PC and polyester segments, respectively. The corresponding asynchronous 2D correlation maps of these four copolymers are shown in Figure S4; the asynchronous map of copolymers features the negative cross-peak in the bottom right (intra-HB C═O vs free C═O) that exhibits a similar behavior in the synchronous map; moreover, intra H-bonding C═O was altered prior to free C═O as the temperature increased,[47] indicating that the intramolecular hydrogen-bonding interaction was more sensitive than that of dipole–dipole interactions or free C═O units as expected.

Analyses of PVPh/CO_2-Based Copolymers Binary Blends. In a previous work,[35] we observed that the binary blends of PVPh/PCHC displayed miscible behavior, because of the intermolecular hydrogen bonding between OH units of PVPh and C═O units of PCHC. Due to the strong intramolecular hydrogen bonding of pure PCHC, the relatively weaker intermolecular hydrogen bonding in PVPh/PCHC binary blends was induced. The K_A < 5 was determined based on the PCAM, and the q value of PVPh/PCHC binary blend was −108 based on the Kwei equation,[35] both suggesting the relatively weaker intermolecular hydrogen bonding in PVPh/PCHC. Through the design of chemical structures of CO_2-based copolymers, the PVPh binary blends with PE-CHA, PCHC-CHA, and PCHC-PA copolymers were investigated in this work.

DSC analysis presented a single T_g value of PVPh/PCHC, PVPh/PE-CHA, PVPh/PCHC-CHA, and PVPh/PCHC-PA binary blends (Figures S5 and 5A,D,G), which indicated that all the copolymers and the PVPh are miscible. Furthermore, the Kwei equation was employed to predict the strength of hydrogen bonding of these miscible binary blending systems, as illustrated in Figure 5B,E,H. The intramolecular hydrogen bonding in PE-CHA is less stable than that in PCHC, resulting in weaker intramolecular hydrogen bonds in PE-CHA compared to those in PCHC (Scheme 2). Consequently, the q value in the Kwei equation for PVPh/PE-CHA binary blends is higher than that for PVPh/PCHC,[35] as shown in Figures 5A and S5. The higher q value for the PVPh/PE-CHA binary blends indicates that it is easier to form intermolecular hydrogen bonding with PVPh in this blending system compared to PVPh/PCHC. The same phenomenon also can be observed in PVPh/PCHC-CHA and PVPh/PCHC-PA binary blending systems (Figure 5E,H), where the q value became −60 and −100, respectively, when the copolymer contains the polyester segment. The q value of these two systems is higher than that of the PVPh/PCHC binary blends.

However, the q value of PVPh/PCHC-PA showed a slight increase compared to PVPh/PCHC. This is due to the π resonance within the aromatic ring, which stabilizes the structure and makes it difficult for electrons to form the

https://doi.org/10.1021/acs.macromol.4c02295
Macromolecules 2025, 58, 1090−1102

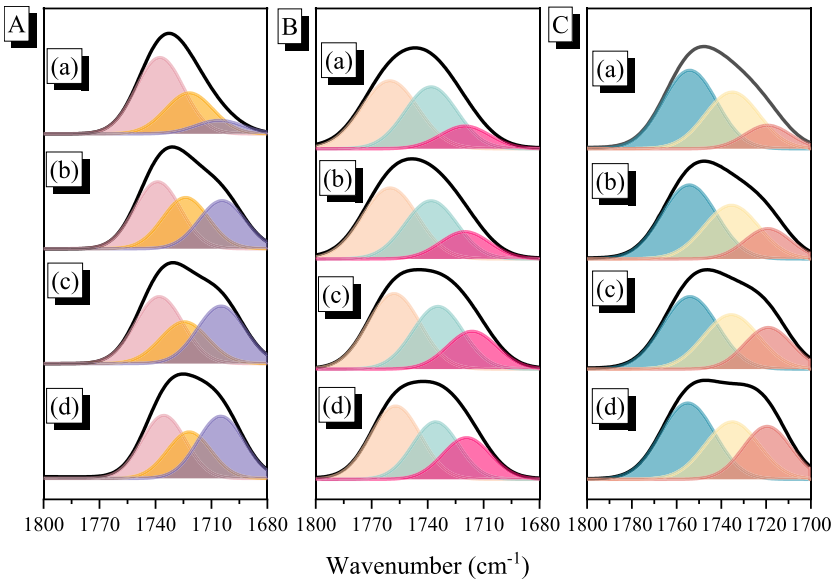

Figure 6. Curve fitting results of the C═O absorptions of selected PVPh/copolymer binary blends including (A) PVPh/PE-CHA100, (B) PVPh/PCHC-CHA100, and (C) PVPh/PCHC-PA100; the different ratio of PVPh/copolymer: (a) 35/65, (b) 50/50, (c) 65/35, and (d) 80/20 blends.

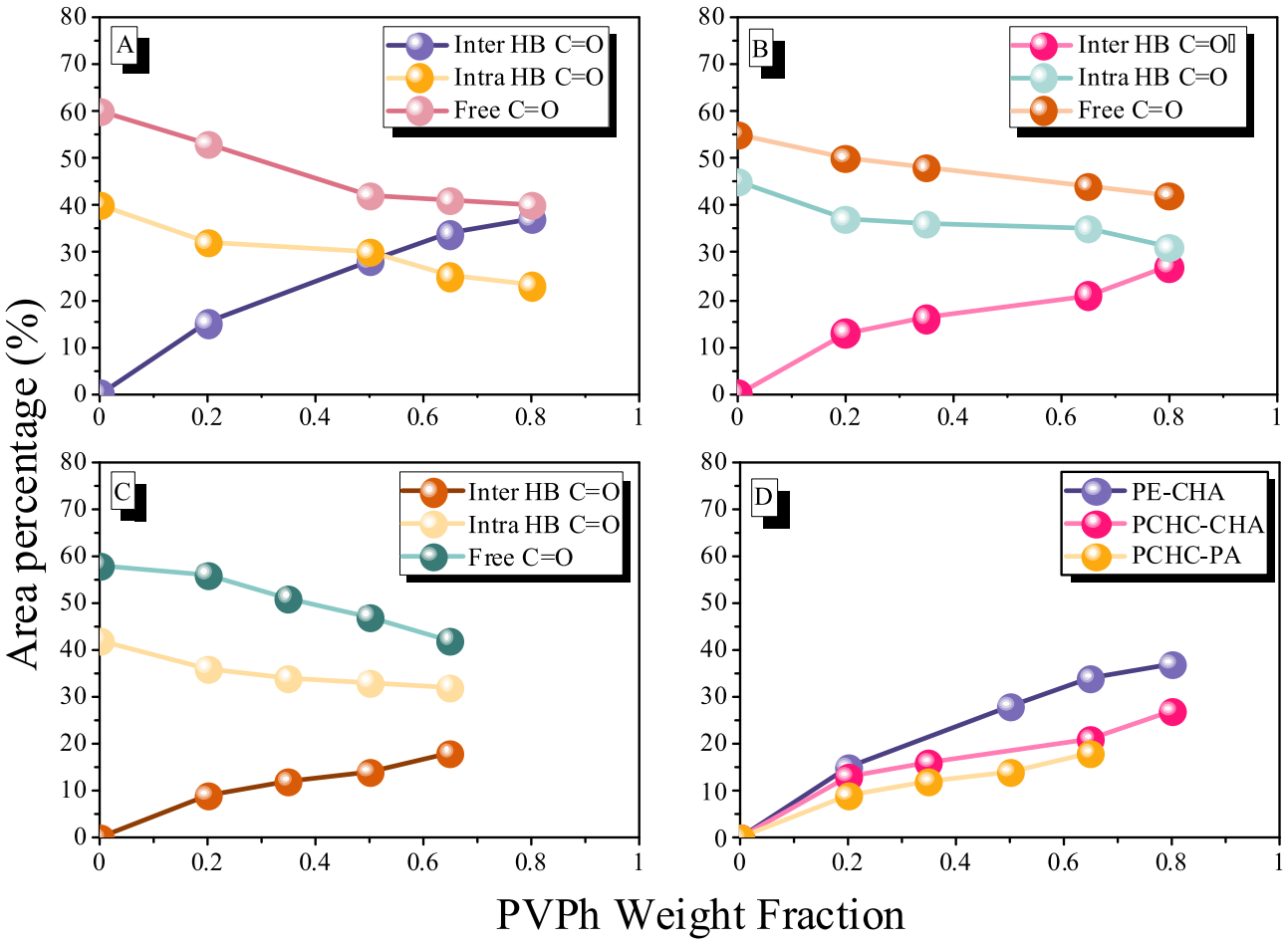

Figure 7. Area fractions of the free C═O, intramolecular, and intermolecular H-bonding C═O units in PVPh/copolymer blends of (A) PE-CHA100, (B) PCHC-CHA100, (C) PCHC-PA100, and (D) area fractions of intermolecular H-bonding C═O units in PVPh/copolymer binary blends.

intermolecular hydrogen bonding with the hydrogen bonding donor, PVPh. Furthermore, phase separation occurred when PCHC-CHA200 was blended with PVPh (Figure S6). This phase separation can be attributed to the blocky segments of the copolymer, which leads to competitive hydrogen bonding between the two segments, the PC and the polyester,

https://doi.org/10.1021/acs.macromol.4c02295
Macromolecules 2025, 58, 1090−1102

particularly if the polyester segment reaches a sufficient proportion within the polymer chain.[55]

As shown in Figure S7, the FTIR spectra revealed the presence of OH stretching absorption in the binary blends, indicating that pure PVPh exhibited two absorption peaks: one for self-associated OH units at 3385 cm^{-1} and another for free OH units at 3540 cm^{-1}. Generally, as the concentration of copolymers in the binary blends increased, the intensity of the free OH units decreased, while the self-associated OH···OH units shifted to relatively higher wavenumbers. This suggests a rearrangement from stronger self-associated OH···OH units to weaker interassociated OH···O=C units. Figure 5C,F,I also indicates that the peak of C=O shifts to a lower wavenumber as the fraction of the PVPh increases. To clarify the change between free and hydrogen bond C=O clearly, and to quantity the fraction of intermolecular hydrogen-bonded C=O units in PVPh/copolymers blends, the peaks of C=O of these three binary blend systems were assigned, the selected curve fitting results are shown in Figure 6, and the fraction of the intermolecular hydrogen-bonded C=O units are summarized in Figure 7.

Figure 7 summarizes the area fractions of the free, intra-, and intermolecular hydrogen bonded C=O units of all PVPh/copolymers binary blend. In general, the fraction of free and intramolecular hydrogen-bonded C=O units decreased as the fraction of PVPh increased (Figure 7A−C); in contrast, the fraction of hydrogen-bonded C=O units was increased for all PVPh/copolymers binary blends as PVPh compositions increased (Figure 7D).

To determine the intermolecular association equilibrium constant (K_A) for all PVPh/copolymers binary blends in this work, see Figure S8; it displays the plots of experimental results and theoretical predictions based on PCAM for each PVPh binary blends determined at 25 °C. The corresponding thermodynamic parameters including molecular weight of repeating unit, molar volume, solubility parameter, and self-association equilibrium constant (K_B) values used are determined in Table 2. The intermolecular hydrogen bonding

Table 2. Thermodynamic Parameters of PVPh/Copolymer Binary Blends Used in This Study at Room Temperature

polymers	molar volume (mL/mol)	molecular weight of repeat unit (g/mol)	solubility parameter (cal/mL)	equilibrium constant	
				K_B	K_A
PVPh	100.0	120	10.6	66.8	
PCHC	94.5	142	10.2		<5
PE-CHA	179.2	252	10.8		11
PCHC-CHA	307.5	394	9.9		6
PCHC-PA	285.1	388	10.6		5

strength in binary blends was in the order of PVPh/PE-CHA (K_A = 11, q = −20), PVPh/PCHC-CHA (K_A = 6, q = −30), PVPh/PCHC-PA (K_A = 5, q = −100), and PVPh/PCHC (K_A < 5, q = −108), which was consistent with DSC analyses based on the order of q values from the Kwei equation. In addition, the K_A values were smaller than the K_B value for pure PVPh, indicating the weaker intermolecular hydrogen bonding in binary blends than that of stronger self-association OH units for PVPh, which would induce the OH units of PVPh, which were shifted to a higher wavenumber and exhibited negative q values based on the Kwei equation.[48]

In addition, the intermolecular hydrogen bonding was also sensitive to temperature change. The PVPh/PCHC-CHA = 65/35 binary blend was chosen to understand the corresponding interaction change, as shown in Figure 8. The signals of OH and C=O units were changed upon increasing temperature, the OH units were significantly shifted to a higher wavenumber (Figure 8A), and the intermolecular hydrogen bonding C=O units were slightly shifted to higher wavenumber (Figure 8B), implying that the hydrogen bonding of OH groups and C=O units were broken as the temperature changed from 60 to 180 °C. Furthermore, the OH absorption was more sensitive than the C=O in binary blend as temperature increased, as shown by 1D FTIR analyses. To analyze the changes in the H-bonding interaction of the binary blends easily, the synchronous 2D-FTIR correlation map was employed (Figure 8C,D). The synchronous correlation spectrum reveals the OH unit in the region of 3000−3700 cm^{-1}, the free OH signal was located at ca. 3580 cm^{-1}, and the hydrogen-bonded OH signal of 3100−3500 cm^{-1} and the center at ca. 3350 cm^{-1} were observed (Figure 8C). Therefore, the C=O unit region of 1700−1800 cm^{-1}, the free C=O signal of 1760 cm^{-1}, the hydrogen-bonded C=O signal of 1710−1740 cm^{-1}, and the center at 1720 cm^{-1} were noticed. Herein, we expected that the hydrogen-bonded C=O was complicated because it should include both intra- and intermolecular hydrogen-bonded C=O units of polycarbonate and polyester segments, and it was still difficult to exhibit each signal in the 2D-FTIR synchronized map. The signal was divided into free C=O and H-bonding C=O units in the 2D-FTIR correlation map. The band of free C=O unit (1760 cm^{-1}) showed positive correlation (red color) with that of the free OH unit (3580 cm^{-1}), and the band of hydrogen-bonded C=O unit (1720 cm^{-1}) showed positive correlation (red color) with that of the hydrogen-bonded OH unit (3350 cm^{-1}). On the contrary, the band of the free C=O unit (1760 cm^{-1}) was negatively correlated (blue color) with that of the hydrogen-bonded C=O unit (1720 cm^{-1}) and hydrogen-bonded OH unit (3350 cm^{-1}). This result means that the negative cross-peaks of free and hydrogen-bonded C=O or OH units would change in opposite directions as the temperature increased. Furthermore, the signal of hydrogen bonding C=O units would be affected by temperature perturbation compared to that of free C=O units, as displayed in Figure 8D. After the temperature increase, the band for hydrogen-bonded C=O units not only significantly decreased but also shifted to a higher wavenumber, while the free C=O unit was almost unchanged.

Figures 9 and S9 exhibit PVPh/PE-CHA = 50/50 and PVPh/PCHC-PA = 50/50 blends of the 2D-FTIR correlation map. The synchronous correlation map of PVPh/PE-CHA blends could be observed, and the signal of C=O was broad and shifted to the lower wavenumber, indicating intermolecular hydrogen bonding appeared between PE-CHA or PCHC-PA and PVPh (Figure 9A,B). Furthermore, we could obtain the relationship from synchronous and asynchronous maps of PE-CHA or PCHC-PA blend with PVPh. As the temperature increased, the order of change of signal was hydrogen-bonded C=O > hydrogen-bonded OH > free OH > free C=O.

The solid state ^{13}C NMR determined the H-bonding interaction between PVPh and copolymers, and the simulated spectra of the blend systems (dashed lines)[56] was obtained by summing the experimental data for PVPh and copolymers at the blend composition based on Figures 10 and S10. It reveals

https://doi.org/10.1021/acs.macromol.4c02295
Macromolecules 2025, 58, 1090−1102

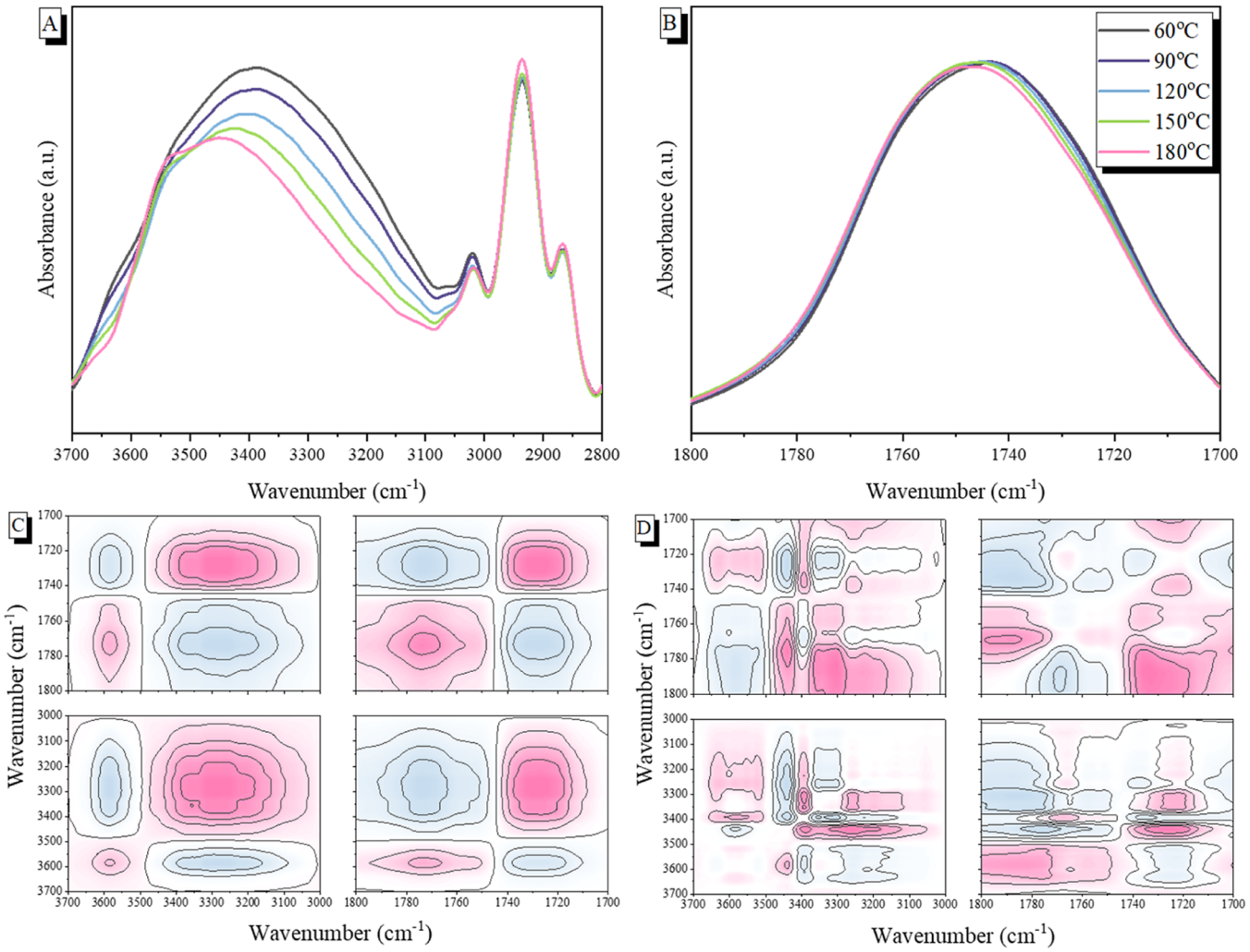

Figure 8. FTIR spectra of the PVPh/PCHC-CHA100 = 65/35 blend, recorded at different temperatures of (A) OH and (B) C═O units and their corresponding 2D-FTIR spectra of (C) synchronous and (D) asynchronous correlation maps.

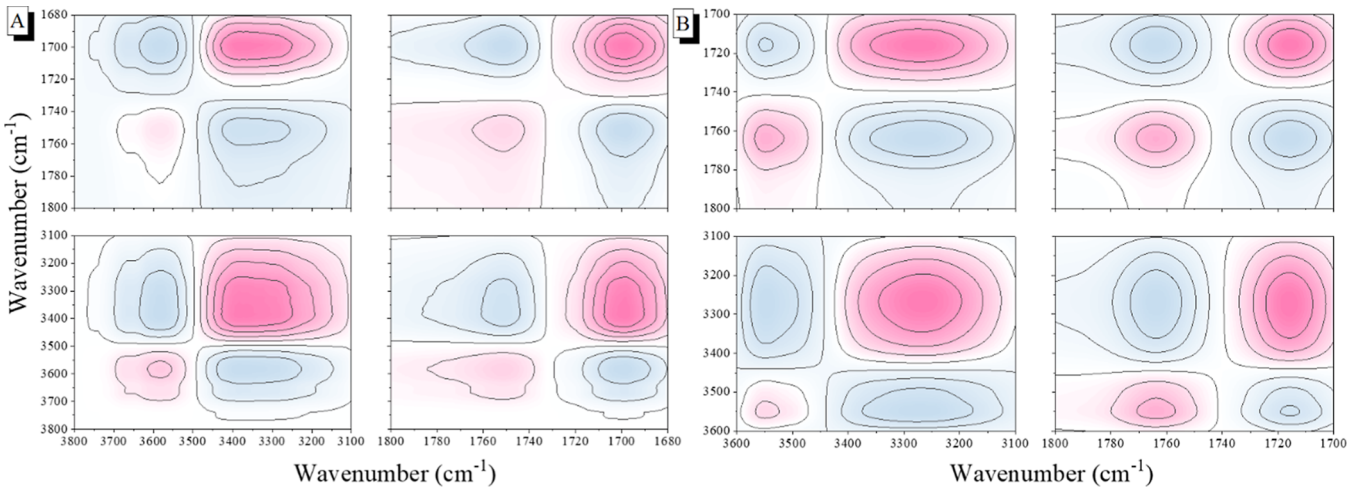

Figure 9. 2D FTIR synchronous spectra of (A) PVPh/PE-CHA100 = 50/50, and (B) PVPh/PCHC-PA100 = 50/50 blends.

that the signal for the C═O carbon nuclei of polycarbonate units shifted to a higher chemical shift slightly, which is the result of intermolecular hydrogen bonding of the C═O groups. In addition, it was also observed that the signal for the C═O carbon nuclei of polyester units shifted to a higher chemical shift (Figure S11). Overall, we concluded that the intermolecular hydrogen bonded strength in binary blends was in the order of PVPh/PE-CHA > PVPh/PCHC-CHA > PVPh/PCHC-PA > PVPh/PCHC binary blends, as summarized in Scheme 3.

https://doi.org/10.1021/acs.macromol.4c02295
Macromolecules 2025, 58, 1090−1102

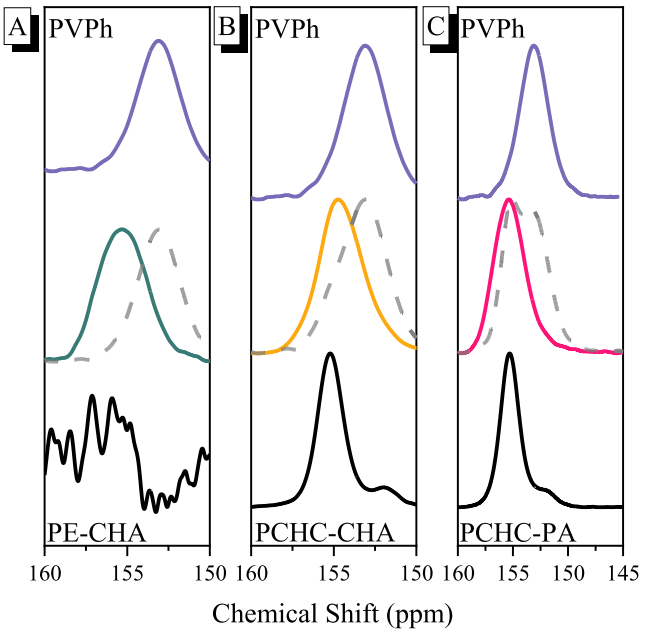

Figure 10. Selected carbon nuclei in solid state ^{13}C NMR spectra, C–OH, and C=O carbon nuclei of PVPh and polycarbonate unit: (A) PVPh/PE-CHA100 = 50/50, (B) PVPh/PCHC-CHA100 = 65/35, and (C) PVPh/PCHC-PA100 = 50/50.

CONCLUSIONS

We successfully prepared CO_2-based polycarbonates by one-pot terpolymerization of CO_2, CHO, and anhydrides with $LZn_2(OAc)_2$ as a catalyst. The aliphatic CHA displays higher reactivity than aromatic PA, and PCHC-CHA has less PCHO units. The introduction of anhydride monomers could form a polyester segment, which exhibits relatively weaker intramolecular hydrogen bonding compared with the polycarbonate segment, and thus the K_A value of PVPh/PE-CHA was higher than that of PVPh/PCHC binary blends. Based on this result, the PVPh/PCHC-CHA and PVPh/PCHC-PA binary blends feature a stronger intermolecular hydrogen bonding rather than PVPh/PCHC binary blend because of the presence of polyester segments in these copolymers. In addition, the PCHC-PA segment induced a more stable structure through the π resonance from aromatic rings, and the intermolecular hydrogen bonding of PVPh/PCHC-PA blend was weaker. Overall, the order of intermolecular hydrogen bonded strength was PVPh/PE-CHA > PVPh/PCHC-CHA > PVPh/PCHC-PA > PVPh/PCHC binary blends. This work provides a general approach to mediate the intra-/intermolecular hydrogen bonding, miscibility behavior, and thermal properties of CO_2-based polycarbonate.

ASSOCIATED CONTENT

Supporting Information

The Supporting Information is available free of charge at https://pubs.acs.org/doi/10.1021/acs.macromol.4c02295.

Characterization methods, GPC, 1D and 2D-FITR, solid state NMR analyses of PVPh/copolymers blends, and inter-association equilibrium constant determined (PDF)

AUTHOR INFORMATION

Corresponding Author

Shiao-Wei Kuo – *Department of Materials and Optoelectronic Science, Center for Functional Polymers and Supramolecular Materials, National Sun Yat-Sen University, Kaohsiung 80424, Taiwan;* orcid.org/0000-0002-4306-7171; Email: kuosw@faculty.nsysu.edu.tw

Authors

Yen-Ling Kuan – *Department of Materials and Optoelectronic Science, Center for Functional Polymers and Supramolecular Materials, National Sun Yat-Sen University, Kaohsiung 80424, Taiwan*

Chih-Wei Chu – *Department of Materials and Optoelectronic Science, Center for Functional Polymers and Supramolecular Materials, National Sun Yat-Sen University, Kaohsiung 80424, Taiwan*

Wei-Ting Du – *Department of Materials and Optoelectronic Science, Center for Functional Polymers and Supramolecular Materials, National Sun Yat-Sen University, Kaohsiung 80424, Taiwan*

Complete contact information is available at: https://pubs.acs.org/10.1021/acs.macromol.4c02295

Author Contributions

The manuscript was written through contributions of all authors.

Scheme 3. Inter/Self-Association Strength of PVPh/Copolymers Binary Blends

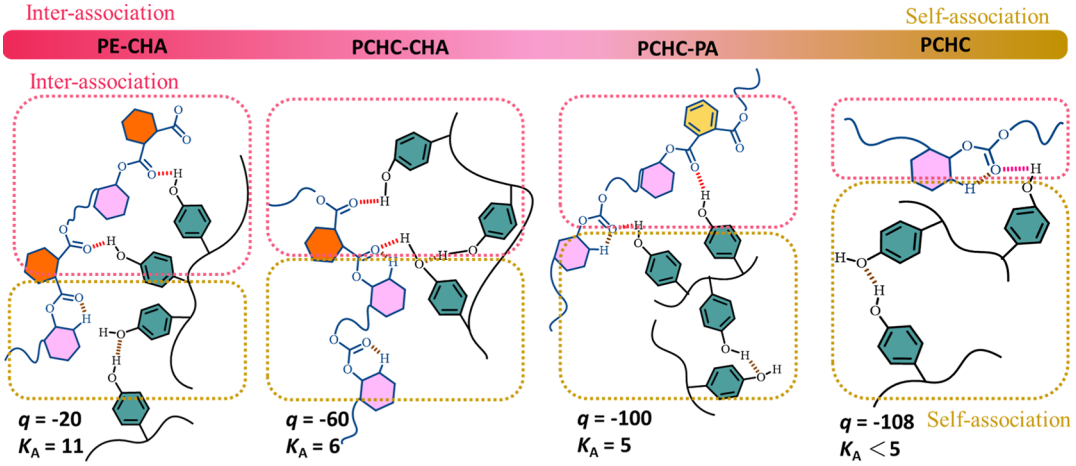

https://doi.org/10.1021/acs.macromol.4c02295
Macromolecules 2025, 58, 1090–1102

Notes

The authors declare no competing financial interest.

■ ACKNOWLEDGMENTS

This study was supported financially by the National Science and Technology Council, Taiwan, under contracts NSTC 112-2218-E-110-007, and 113-2218-E-110-004.

■ REFERENCES

(1) Deacy, A. C.; Durr, C. B.; Garden, J. A.; White, A. J. P.; Williams, C. K. Groups 1, 2 and Zn(II) Heterodinuclear Catalysts for Epoxide/CO_2 Ring-Opening Copolymerization. *Inorg. Chem.* **2018**, *57*, 15575−15583.
(2) Stegmann, P.; Daioglou, V.; Londo, M.; van Vuuren, D. P.; Junginger, M. Plastic futures and their CO_2 emissions. *Nature* **2022**, *612*, 272−276.
(3) Muthuraj, R.; Mekonnen, T. Recent progress in carbon dioxide (CO_2) as feedstock for sustainable materials development: Co-polymers and polymer blends. *Polymer* **2018**, *145*, 348−373.
(4) Geyer, R.; Jambeck, J. R.; Law, K. L. Production, use, and fate of all plastics ever made. *Sci. Adv.* **2017**, *3*, 25−29.
(5) de Oliveira, C. C. N.; Zotin, M. Z.; Rochedo, P. R. R.; Szklo, A. Achieving negative emissions in plastics life cycles through the conversion of biomass feedstock. *Biofuel. Bioprod. Biorefin.* **2021**, *15*, 430−453.
(6) Thomas, C. M. Stereocontrolled ring-opening polymerization of cyclic esters: synthesis of new polyester microstructures. *Chem. Soc. Rev.* **2010**, *39*, 165−173.
(7) Diaz, C.; Mehrkhodavandi, P. Strategies for the synthesis of block copolymers with biodegradable polyester segments. *Polym. Chem.* **2021**, *12*, 783−806.
(8) Fukushima, K.; Nozaki, K. Organocatalysis: A Paradigm Shift in the Synthesis of Aliphatic Polyesters and Polycarbonates. *Macromol.* **2020**, *53*, 5018−5022.
(9) Zhang, J.; Wang, L.; Liu, S.; Kang, X.; Li, Z. A Lewis Pair as Organocatalyst for One-Pot Synthesis of Block Copolymers from a Mixture of Epoxide, Anhydride, and CO_2. *Macromol.* **2021**, *54*, 763−772.
(10) Paul, S.; Zhu, Y.; Romain, C.; Brooks, R.; Saini, P. K.; Williams, C. K. Ring-opening copolymerization (ROCOP): synthesis and properties of polyesters and polycarbonates. *Chem. Commun.* **2015**, *51*, 6459−6479.
(11) Longo, J. M.; Sanford, M. J.; Coates, G. W. Ring-Opening Copolymerization of Epoxides and Cyclic Anhydrides with Discrete Metal Complexes: Structure-Property Relationships. *Chem. Rev.* **2016**, *116*, 15167−15197.
(12) van Heek, J.; Arning, K.; Ziefle, M. Reduce, reuse, recycle: Acceptance of CO_2-utilization for plastic products. *Energy Policy* **2017**, *105*, 53−66.
(13) Tang, S.; Nozaki, K. Advances in the Synthesis of Copolymers from Carbon Dioxide, Dienes, and Olefins. *Acc. Chem. Res.* **2022**, *55*, 1524−1532.
(14) Deacy, A. C.; Moreby, E.; Phanopoulos, A.; Williams, C. K. Co(III)/Alkali-Metal(I) Heterodinuclear Catalysts for the Ring-Opening Copolymerization of CO_2 and Propylene Oxide. *J. Am. Chem. Soc.* **2020**, *142*, 19150−19160.
(15) Qiu, L. Q.; Li, H. R.; He, L. N. Incorporating Catalytic Units into Nanomaterials: Rational Design of Multipurpose Catalysts for CO_2 Valorization. *Acc. Chem. Res.* **2023**, *56* (16), 2225−2240.
(16) Du, W. T.; Chen, S. Y.; Kuo, S. W. Mesoporous phenolic/carbon materials templated by CO2-based PEO-b-PCHC diblock copolymers through mediated competitive intermolecular hydrogen bonding interactions for CO2 capture. *J. CO2 Util.* **2024**, *80*, 102702.
(17) Mohamed, M. G.; Chang, W. C.; Kuo, S.-W. Crown Ether- and Benzoxazine-Linked Porous Organic Polymers Displaying Enhanced Metal Ion and CO2 Capture through Solid-State Chemical Transformation. *Macromol.* **2022**, *55*, 7879−7892.
(18) Ejaz, M.; Mohamed, M. G.; Kuo, S. W. Solid state chemical transformation provides a fully benzoxazine-linked porous organic polymer displaying enhanced CO_2 capture and supercapacitor performance. *Polym. Chem.* **2023**, *14*, 2494−2509.
(19) Mohamed, M. G.; Chang, S.-Y.; Ejaz, M.; Samy, M. M.; Mousa, A. O.; Kuo, S.-W. Design and Synthesis of Bisulfone-Linked Two-Dimensional Conjugated Microporous Polymers for CO_2 Adsorption and Energy Storage. *Molecules* **2023**, *28*, 3234.
(20) Mousa, A. O.; Mohamed, M. G.; Chuang, C. H.; Kuo, S. W. Carbonized Aminal-Linked Porous Organic Polymers Containing Pyrene and Triazine Units for Gas Uptake and Energy Storage. *Polymers* **2023**, *15*, 1891.
(21) Hepburn, C.; Adlen, E.; Beddington, J.; Carter, E. A.; Fuss, S.; Mac Dowell, N.; Minx, J. C.; Smith, P.; Williams, C. K. The technological and economic prospects for CO_2 utilization and removal. *Nature* **2019**, *575*, 87−97.
(22) Wang, Y.; Darensbourg, D. J. Carbon dioxide-based functional polycarbonates: Metal catalyzed copolymerization of CO_2 and epoxides. *Coord. Chem. Rev.* **2018**, *372*, 85−100.
(23) Plajer, A. J.; Williams, C. K. Heterotrinuclear Ring-Opening Copolymerization Catalysis: Structure-Activity Relationships. *ACS Catal.* **2021**, *11*, 14819−14828.
(24) Xu, Y.; Lin, L.; Xiao, M.; Wang, S.; Smith, A. T.; Sun, L.; Meng, Y. Synthesis and properties of CO_2-based plastics: Environmentally-friendly, energy-saving and biomedical polymeric materials. *Prog. Polym. Sci.* **2018**, *80*, 163−182.
(25) Tu, Z.; Lu, Y.; Sang, L.; Zhang, Y.; Li, Y.; Wei, Z. Kilogram-Scale Preparation of Poly(ethylene oxalate) toward Marine-Degradable Plastics. *Macromol.* **2023**, *56* (8), 3149−3159.
(26) Omura, K.; Aiba, Y.; Suzuki, K.; Ariyasu, S.; Sugimoto, H.; Shoji, O. A P450 harboring manganese protoporphyrin IX generates a manganese analogue of compound I by activating dioxygen. *ACS Catal.* **2022**, *12*, 11108−11117.
(27) Han, B.; Liu, B.; Ding, H.; Duan, Z.; Wang, X.; Theato, P. CO_2-Tuned Sequential Synthesis of Stereoblock Copolymers Comprising a Stereoregularity-Adjustable Polyester Block and an Atactic CO_2-Based Polycarbonate Block. *Macromol.* **2017**, *50*, 9207−9215.
(28) Inoue, S.; Koinuma, H.; Tsuruta, T. Copolymerization of carbon dioxide and epoxide. *J. Polym. Sci., Polym. Lett.* **1969**, *7*, 287−292.
(29) Inoue, S.; Koinuma, H.; Tsuruta, T. Copolymerization of carbon dioxide and epoxide with organometallic compounds. *Makromol. Chem.* **1969**, *130*, 210−220.
(30) Li, Y.; Shimizu, H. Compatibilization by Homopolymer: Significant Improvements in the Modulus and Tensile Strength of PPC/PMMA Blends by the Addition of a Small Amount of PVAc. *ACS Appl. Mater. Interfaces* **2009**, *1*, 1650−1655.
(31) Song, L.; Li, Y.; Meng, X.; Wang, T.; Shi, Y.; Wang, Y.; Shi, S.; Liu, L.-Z. Crystallization, Structure and Significantly Improved Mechanical Properties of PLA/PPC Blends Compatibilized with PLA-PPC Copolymers Produced by Reactions Initiated with TBT or TDI. *Polymers* **2021**, *13*, 3245.
(32) Zuo, H.; Liu, J.; Huang, D.; Bai, Y.; Cui, L.; Pan, L.; Zhang, K.; Wang, H. Sustainable and high-performance ternary blends from polylactide, CO_2-based polyester and microbial polyesters with different chemical structure. *J. Polym. Sci.* **2021**, *59*, 1578−1595.
(33) Dong, X.; Liu, L.; Wang, Y.; Li, T.; Wu, Z.; Yuan, H.; Ma, P.; Shi, D.; Chen, M.; Dong, W. The compatibilization of poly (propylene carbonate)/poly (lactic acid) blends in presence of core-shell starch nanoparticles. *Carbohydr. Polym.* **2021**, *254*, 117321.
(34) Yu, T.; Zhou, Y.; Zhao, Y.; Liu, K. P.; Chen, E. Q.; Wang, D. J.; Wang, F. S. Hydrogen-bonded thermostable liquid crystalline complex formed by biodegradable polymer and amphiphilic molecules. *Macromol.* **2008**, *41*, 3175−3180.
(35) Du, W. T.; Kuan, Y. L.; Kuo, S. W. Intra- and Intermolecular Hydrogen Bonding in Miscible Blends of CO_2/Epoxy Cyclohexene Copolymer with Poly(Vinyl Phenol). *Int. J. Mol. Sci.* **2022**, *23*, 7018.
(36) Kuan, Y. L.; Du, W. T.; Kuo, S. W. Effect of polyhedral oligomeric silsesquioxane (POSS) nanoparticle on the miscibility and

https://doi.org/10.1021/acs.macromol.4c02295
Macromolecules 2025, 58, 1090−1102

hydrogen bonding behavior of CO_2 based poly(cyclohexene carbonate) copolymers. *J. Taiwan Inst. Chem. Eng.* **2023**, *153*, 105214.
(37) Zhao, J. Q.; Pearce, E. M.; Kwei, T. K. Binary and ternary blends of polystyrene-block-poly(p-hydroxystyrene). *Macromol.* **1997**, *30*, 7119−7126.
(38) Yang, Z.; Han, C. D. Rheology of Miscible Polymer Blends with Hydrogen Bonding. *Macromol.* **2008**, *41*, 2104−2118.
(39) Kang, S.; Lee, J.; Kim, E.; Seo, Y.; Choi, C.; Kim, J. K. Inverted Cylindrical Microdomains from Binary Block Copolymer Blends Capable of Hydrogen Bonding. *Macromol.* **2021**, *54*, 8971−8976.
(40) Kulshreshtha, A.; Hayward, R. C.; Jayaraman, A. Impact of Composition and Placement of Hydrogen-Bonding Groups along Polymer Chains on Blend Phase Behavior: Coarse-Grained Molecular Dynamics Simulation Study. *Macromol.* **2022**, *55*, 2675−2690.
(41) Du, M. X.; Yuan, Y. F.; Zhang, J. M.; Liu, C. Y. Hydrogen-Bonding Interactions in Polymer-Organic Solvent Mixtures. *Macromol.* **2022**, *55*, 4578−4588.
(42) Tsou, C. T.; Kuo, S. W. Competing Hydrogen Bonding Interaction Creates Hierarchically Ordered Self-Assembled Structures of PMMA-b-P4VP/PVPh-b-PS Mixtures. *Macromol.* **2019**, *52*, 8374−8383.
(43) Chen, W. C.; Kuo, S. W.; Jeng, U. S.; Chang, F. C. Self-assembly through competitive interactions of miscible diblock copolymer/homopolymer blends: Poly (vinylphenol-b-methyl methacrylate)/poly (vinylpyrrolidone) blend. *Macromol.* **2008**, *41*, 1401−1410.
(44) Lin, C. L.; Chen, W. C.; Liao, C. S.; Su, Y. C.; Huang, C. F.; Kuo, S. W.; Chang, F. C. Sequence distribution and polydispersity index affect the hydrogen-bonding strength of poly (vinylphenol-co-methyl methacrylate) copolymers. *Macromol.* **2005**, *38*, 6435−6444.
(45) Kuo, S. W.; Tung, P. H.; Chang, F. C. Syntheses and the study of strongly hydrogen-bonded poly (vinylphenol-b-vinylpyridine) diblock copolymer through anionic polymerization. *Macromol.* **2006**, *39*, 9388−9395.
(46) Tsai, S. C.; Lin, Y. C.; Lin, E. L.; Chiang, Y. W.; Kuo, S. W. Hydrogen bonding strength effect on self-assembly supramolecular structures of diblock copolymer/homopolymer blends. *Polym. Chem.* **2016**, *7*, 2395−2409.
(47) Noda, I. Two-Dimensional Infrared Spectroscopy. *J. Am. Chem. Soc.* **1989**, *111*, 8116−8118.
(48) Coleman, M. M.; Painter, P. C. Hydrogen Bonded Polymer Blends. *Prog. Polym. Sci.* **1995**, *20*, 1−59.
(49) Kwei, T. K. The effect of hydrogen bonding on the glass transition temperatures of polymer mixtures. *J. Polym. Sci., Polym. Lett. Ed.* **1984**, *22*, 307−313.
(50) Sun, X.-K.; Zhang, X.-H.; Chen, S.; Du, B.-Y.; Wang, Q.; Fan, Z.-Q.; Qi, G.-R. One-Pot Terpolymerization of CO_2, Cyclohexene Oxide and Maleic Anhydride Using a Highly Active Heterogeneous Double Metal Cyanide Complex Catalyst. *Polymer* **2010**, *51*, 5719−5725.
(51) Romain, C.; Zhu, Y.; Dingwall, P.; Paul, S.; Rzepa, H. S.; Buchard, A.; Williams, C. K. Chemoselective Polymerizations from Mixtures of Epoxide, Lactone, Anhydride, and Carbon Dioxide. *J. Am. Chem. Soc.* **2016**, *138*, 4120−4131.
(52) Kummari, A.; Pappuru, S.; Chakraborty, D. Fully Alternating and Regioselective Ring-Opening Copolymerization of Phthalic Anhydride with Epoxides Using Highly Active Metal-Free Lewis Pairs as a Catalyst. *Polym. Chem.* **2018**, *9*, 4052−4062.
(53) Xu, Y. H.; Wang, S. J.; Lin, L.; Xiao, M.; Meng, Y. Z. Semi-crystalline terpolymers with varying chain sequence structures derived from CO_2, cyclohexene oxide and ϵ-caprolactone: one-step synthesis catalyzed by tri-zinc complexes. *Polym. Chem.* **2015**, *6*, 1533.
(54) Xu, Y. H.; Zhang, T.; Zhou, Y.; Zhou, D.; Shen, Z.; Lin, L. Mechanism investigation of thermal degradation of CO_2-based poly(cyclohexene carbonate caprolactone). *Polym. Degrad. Stab.* **2019**, *168*, 108957.
(55) Kuo, S. W. *Hydrogen Bonding in Polymer Materials*; John Wiley & Sons: Hoboken, NJ, 2018.
(56) Asano, A.; Eguchi, M.; Shimizu, M.; Kurotsu, T. Miscibility and Molecular Motion of PMAA/PVAc Blends Investigated by High-Resolution Solid-State CPMAS ^{13}C NMR. *Macromol.* **2002**, *35*, 8819−8824.

https://doi.org/10.1021/acs.macromol.4c02295
Macromolecules 2025, 58, 1090−1102